NAVAL POSTGRADUATE SCHOOL

MONTEREY, CALIFORNIA

THESIS

CONTINUUM MODELING OF INTERFACE FAILURE

by

Robert P. Griffiths

December 2007

Thesis Advisor: Young W. Kwon

Approved for public release; distribution is unlimited.

THIS PAGE INTENTIONALLY LEFT BLANK

REPORT DOCUMENTATION PAGE			Form Approved OMB No. 0704-0188
Public reporting burden for this collection of information is estimated to average 1 hour per response, including the time for reviewing instruction, searching existing data sources, gathering and maintaining the data needed, and completing and reviewing the collection of information. Send comments regarding this burden estimate or any other aspect of this collection of information, including suggestions for reducing this burden, to Washington headquarters Services, Directorate for Information Operations and Reports, 1215 Jefferson Davis Highway, Suite 1204, Arlington, VA 22202-4302, and to the Office of Management and Budget, Paperwork Reduction Project (0704-0188) Washington DC 20503.			
1. AGENCY USE ONLY *(Leave blank)*	**2. REPORT DATE** December 2007	**3. REPORT TYPE AND DATES COVERED** Master's Thesis	
4. TITLE AND SUBTITLE Continuum Modeling of Interface Failure			**5. FUNDING NUMBERS**
6. AUTHOR(S) Griffiths, Robert P.			
7. PERFORMING ORGANIZATION NAME(S) AND ADDRESS(ES) Naval Postgraduate School Monterey, CA 93943-5000			**8. PERFORMING ORGANIZATION REPORT NUMBER**
9. SPONSORING /MONITORING AGENCY NAME(S) AND ADDRESS(ES)			**10. SPONSORING/MONITORING AGENCY REPORT NUMBER**
11. SUPPLEMENTARY NOTES The views expressed in this thesis are those of the author and do not reflect the official policy or position of the Department of Defense or the U.S. Government.			
12a. DISTRIBUTION / AVAILABILITY STATEMENT Approved for public release; distribution is unlimited.			**12b. DISTRIBUTION CODE**

13. ABSTRACT (maximum 200 words)

Two-dimensional continuum modeling and simulations were conducted to predict how the size, quantity, and stiffness of reinforcing particles such as carbon nanotubes (CNTs) affect failure mechanisms at the interface of composite structures. First, the strength model used the finite element method (FEM) on a slender composite beam with step-joint containing reinforcing particles to predict its critical stress-strain behavior at the joint interface under compressive axial load. Next, the fracture mechanics model used the virtual crack extension method on the same composite beam containing an internal crack to predict how the energy release rate was affected by reinforcing particles at the interface under the same compressive axial load. Comparing the two results to experimental data showed that the fracture mechanics model predicted the interface failure behavior better than the strength model. Finally, the fracture mechanics model was used for a composite plate containing an edge crack to study how the energy release rate was affected by several parameters of reinforcing particles near the crack tip under transverse shear load. In each case, homogeneous models served as baselines for comparative analyses. Outcome of this work not only represents reliable and efficient modeling of composite interfaces in order to improve failure strength through the addition of nanoscale reinforcing particles such as CNTs but also serves to focus future research in structural application of CNTs, especially within testing and evaluation of CNTs in composite scarf-joint interfaces.

14. SUBJECT TERMS Interface Failure, Fracture Mechanics Modeling, Strength Modeling, Composite Interface, Carbon Nanotubes, Finite Element Method			**15. NUMBER OF PAGES** 55
			16. PRICE CODE
17. SECURITY CLASSIFICATION OF REPORT Unclassified	**18. SECURITY CLASSIFICATION OF THIS PAGE** Unclassified	**19. SECURITY CLASSIFICATION OF ABSTRACT** Unclassified	**20. LIMITATION OF ABSTRACT** UU

NSN 7540-01-280-5500

Standard Form 298 (Rev. 2-89)
Prescribed by ANSI Std. 239-18

THIS PAGE INTENTIONALLY LEFT BLANK

Approved for public release; distribution is unlimited.

CONTINUUM MODELING OF INTERFACE FAILURE

Robert P. Griffiths
Lieutenant, United States Coast Guard
B.S., San Diego State University, 1999

Submitted in partial fulfillment of the
requirements for the degree of

MASTER OF SCIENCE IN MECHANICAL ENGINEERING

from the

NAVAL POSTGRADUATE SCHOOL
December 2007

Author: Robert P. Griffiths

Approved by: Young W. Kwon
Thesis Advisor

Anthony J. Healey
Chairman, Department of Mechanical and Astronautical Engineering

THIS PAGE INTENTIONALLY LEFT BLANK

ABSTRACT

Two-dimensional continuum modeling and simulations were conducted to predict how the size, quantity, and stiffness of reinforcing particles such as carbon nanotubes (CNTs) affect failure mechanisms at the interface of composite structures. First, the strength model used the finite element method (FEM) on a slender composite beam with step-joint containing reinforcing particles to predict its critical stress-strain behavior at the joint interface under compressive axial load. Next, the fracture mechanics model used the virtual crack extension method on the same composite beam containing an internal crack to predict how the energy release rate was affected by reinforcing particles at the interface under the same compressive axial load. Comparing the two results to experimental data showed that the fracture mechanics model predicted the interface failure behavior better than the strength model. Finally, the fracture mechanics model was used for a composite plate containing an edge crack to study how the energy release rate was affected by several parameters of reinforcing particles near the crack tip under transverse shear load. In each case, homogeneous models served as baselines for comparative analyses. Outcome of this work not only represents reliable and efficient modeling of composite interfaces in order to improve failure strength through the addition of nanoscale reinforcing particles such as CNTs but also serves to focus future research in structural application of CNTs, especially within testing and evaluation of CNTs in composite scarf-joint interfaces.

THIS PAGE INTENTIONALLY LEFT BLANK

TABLE OF CONTENTS

LIST OF FIGURES

LIST OF TABLES

I. INTRODUCTION

A. BACKGROUND

Since first being reported by Iijima in 1991 [1], carbon nanotubes (CNTs) have been the subject of widening research in fracture mechanics given their exceptional mechanical properties. With elastic modulus on the order of 1TPa, CNTs have potential for a multitude of structural applications including use as reinforcing particles in polymer matrix composites or perhaps even metal matrix composites in order to enhance the joint-interface fracture toughness [2-3].

A survey of recent work showed classical molecular dynamics (MD) simulations had been used to model elastic and plastic properties of CNTs as well as mechanisms of strain release under various types of loading conditions. In one case [4], MD simulations found CNTs to be exceptionally resilient and able to sustain extreme strain deformation with no signs of brittleness, plasticity, or atomic rearrangements. In another case [5], both MD simulations and experimental testing were combined in continuum modeling that revealed single- and multi-walled CNTs are highly flexible, able to withstand large strains and even bending in excess of 110°. In fact, ref. [6] used MD simulations to perform a comparative analysis of elastic modulus on two common types of nanotubes, suggesting there exists a 58% greater stiffness in single-walled when compared to bamboo structure CNTs,

Remarkable achievements have also been made in the application of CNTs to structures, most notably through CNT-reinforced polymer matrix composites [7-9]. Uniform dispersion within the polymer matrix and wettability remain critical issues. In one experiment [10], the addition of 1 wt. % CNTs to polystyrene resulted in a favorable 42% increase in stiffness as well as a 25% increase in strength. In another experiment [11], a single multi-walled nanotube was embedded in a polymer matrix was found to have very high compressive strength, more than 2 orders of magnitude higher than any known fiber. In fact, ref. [12] dispersed 7.5 g/m^2 of various multi-walled and bamboo CNTs into a composite scarf joints containing vinyl ester matrix and subjected them to

compressive axial loading that resulted in a 26% increase in stiffness as well as an 11% increase in strength on average when compared to similar joints without CNTs.

But while design and fabrication of CNTs is clearly on the nanoscale, there exists a fundamental need for favorable macroscopic results in engineering applications. It is through the use of continuum modeling that the seemingly theoretical design and fabrication of nanoscale particles, such as CNTs, can be readily applied to engineering designs in order to predict macroscopic mechanical behavior of a system. This type of modeling is essential to the development of CNT-reinforced composites.

B. OBJECTIVES

The principal objective of this work is to provide a reliable and efficient method of modeling composite interfaces in order to improve failure strength through the addition of nanometer scale reinforcing particles such as CNTs. To this end, modeling will be performed in order to predict how the size, quantity, and stiffness of reinforcing particles such as CNTs affect failure mechanisms at the interfaces of composite structures. Comparisons will be drawn to recent experimental work in e.g., [12]. The primary goal here is to assist future researchers in any structural application of nanotechnology, especially within the realm of testing and evaluation of CNTs in composite scarf-joint interfaces.

II. CONTINUUM MODELING

A. INTRODUCTION

Two-dimensional modeling can be used to predict the fracture mechanics of composite material reinforced by particles such as carbon nanotubes (CNTs). Varying the size, location, and stiffness of reinforcing particles at the interface causes changes in stress-strain behavior as well as the amount of energy released. Identifying critical values for each helps in the prediction of crack propagation and provides a correlation between the analytical results presented here and, for example, the experimental results obtained in [12].

B. STRENGTH MODEL

The strength model shows how the stress-strain behavior is influenced by the application of reinforcing particles in the matrix material of a composite beam. These analytical predictions are made by calculating the state of stress and strain, and related energies, at the interface in order to predict failure under an applied compressive load.

1. Cantilevered Beam

Consider a composite beam as shown in Figure 1. This slender cantilevered beam comprises three linear isotropic materials having Young's moduli $E_1 = 50GPa$, $E_2 = 8.0GPa$, $E_3 = 400GPa$ and Poisson's ratios $\nu_1 = 0.30$, $\nu_2 = 0.28$, $\nu_3 = 0.20$. Let length $l = 0.62m$ and height $h = 0.05m$. The left edge is clamped while the right edge is subject to compressive force $F_x = 5,000N$ and constrained in the *y*-direction. To control for the effects of bending, surface nodes at the loading point are coupled in the *y*-direction thus preventing the free end from rotating while still allowing for axial displacement.

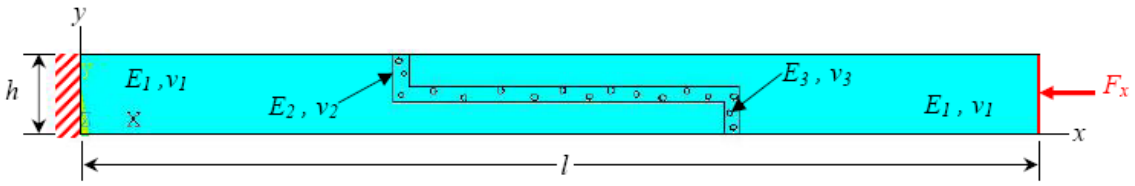

Figure 1. Composite beam under applied compressive load.

2. Critical Load Beam Bending

Using first principles of Euler elastic stability for slender beam to analyze the critical load P_{cr} of the main constituent material

$$P_{cr} = \frac{\pi^2 EI}{L_e^2} = \frac{\pi^2 E_1 \left[lh^3 \right]}{\left[0.7(l) \right]^2} = \frac{\pi^2 \left(50 \cdot 10^9 \right) \left[(0.62)(0.05)^3 \right]}{\left[0.7(0.62) \right]^2} = 203.1 \cdot 10^6 N \qquad (1)$$

where the effective length $L_e = 0.70(l)$ for clamped end, results in $P_{cr} = 203.1 \cdot 10^6 N$, which is substantially greater than the load $P = 5kN$ being applied here thus buckling is not expected [13].

3. FEM Model of Composite Beam

A two-dimensional finite element method (FEM) model in ANSYS uses higher order eight-node element (i.e., PLANE183) having quadratic displacement behavior. Each node has two degrees of freedom, u_x and u_y, with the degenerated element having coincident nodes *K*, *L*, and *O*, as depicted by the shape in Figure 2 [14]. Linear elastic plane stress behavior is assumed for this static analysis.

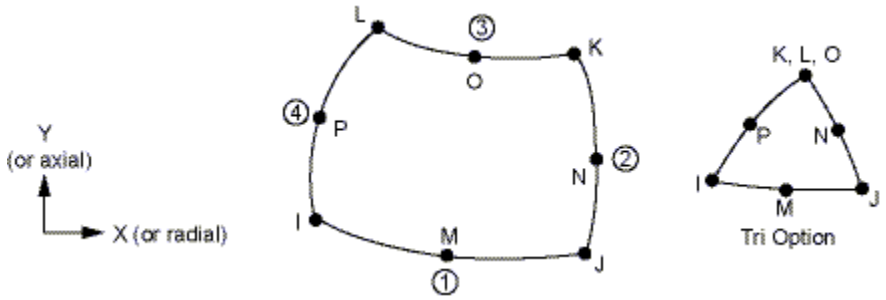

Figure 2. 2-D FEM 8-node structural solid element geometry (PLANE183) [14].

Each area is freely meshed using *smart size* level 1 elements with one subsequent refinement. The right side of the beam has an applied total force load $F_x = -5kN$ distributed to each node and constrained in the *y* direction. The left side of the beam is clamped and therefore constrained in both *x* and *y* directions. See Figure 3.

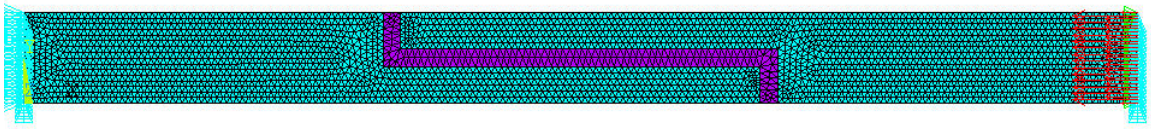

Figure 3. Strength model of composite beam under compressive nodal load.

C. FRACTURE MECHANICS BEAM MODEL

The fracture mechanics beam model shows how an internal crack or flaw in the interface of a composite joint propagates under an applied axial load and how this process is influenced by the application of reinforcing particles such as CNTs. These analytical predictions are made by calculating fracture parameters such as the energy release rate in the region of a crack in order to estimate the crack growth rate. While the energy release rate *G* represents the amount of work associated with a crack opening, it is at the point of instability when the change in potential energy equals the change in the crack length that fracture occurs.

1. Cantilevered Beam with Internal Crack

Consider a composite beam with internal crack as shown in Figure 4. This slender cantilevered beam comprises three linear isotropic materials having Young's moduli $E_1 = 50GPa$, $E_2 = 8.0GPa$, $E_3 = 400GPa$ and Poisson's ratios $\nu_1 = 0.30$, $\nu_2 = 0.28$, $\nu_3 = 0.20$. Let length $l = 0.62m$, height $h = 0.05m$, and crack length $a = 0.01m$. The left edge is clamped while the right edge is subject to compressive force $F_x = 5,000N$ and constrained in the *y*-direction. To control for the effects of bending, surface nodes at the loading point are coupled in the *y*-direction thus preventing the free end from rotating while still allowing for axial displacement.

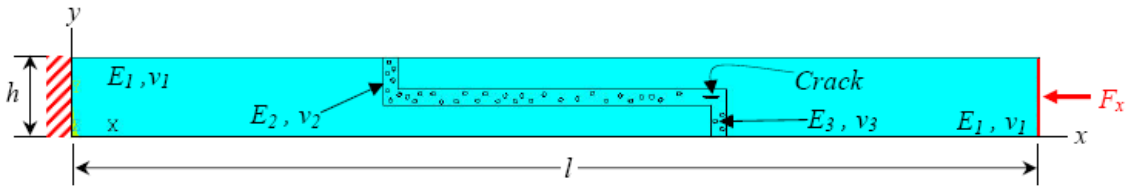

Figure 4. Composite beam with internal crack under applied compressive load.

2. FEM Model of Composite Beam with Internal Crack

The same kind of finite elements used in the strength model are also adopted here except that in the region of the crack tip quarter-point singular eight-node elements (i.e., PLANE183) are used instead. The radius of the first row elements is specified at $a/8 = 1.25mm$ and the second row ratio is set to 50 percent. Linear elastic plane stress behavior is also assumed for this static analysis. A very small opening ($\sim a/200$) facilitates modeling of the crack face.

Each area is freely meshed using *smart size* level 1 elements with one refinement. The right side of the beam has an applied total force load $F_x = -5kN$ distributed to each node, constrained in the *y* direction. The left side of the beam is clamped and therefore constrained in both *x* and *y* directions. See Figure 5.

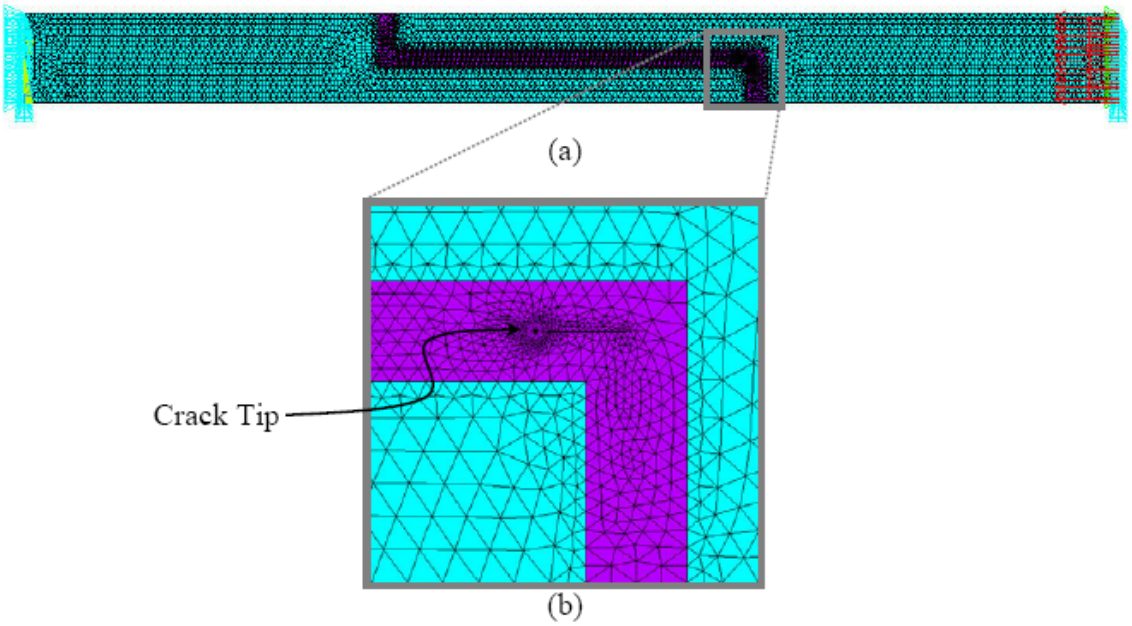

Figure 5. Mesh of fracture mechanics beam model with internal crack (*a*) under compressive nodal force with expanded view of crack tip (*b*).

3. Virtual Crack Extension Method

In the virtual crack extension method, two separate analysis are performed, one before extension with crack length a and the other after extension with crack length $a + \Delta a$.

In the first analysis, before extension, a 2-D FEM model obtains the reaction solution for resultant nodal forces F_x and F_y at the crack tip. In this case, the crack tip is located at node 1412 and therefore F_x and F_y are taken at that node.

Before starting the second analysis, the crack length is extended. Extension of the crack length is carried out by selecting all nodes in the vicinity of the crack tip, which is defined here as all nodes located within radial distance $r = a/2 = 5mm$ of the crack tip, and then the selected nodes are scaled and moved in the negative x direction for a distance equivalent to 1/2 percent of the crack length. This action results in total crack

length extension $\Delta a = 10mm(0.5\%) = 0.05mm$, which corresponds to nodal scaling factor $R_y = 40.495/40.5$. The crack tip remains at node 1412, now at an extended distance from its prior location.

In the second analysis, with crack length extension, a 2-D FEM model obtains the reaction solution for resultant nodal displacement components u_x and u_y at the crack tip. In this case, we take the difference of u_x and u_y between nearest neighboring nodes 1419 and 1421 post-solution, using

$$\Delta u_x = u_{x-N1419} - u_{x-N1421} \tag{2}$$

$$\Delta u_y = u_{y-N1419} - u_{y-N1421} \tag{3}$$

Linear interpolation provides the resultant components of virtual displacement Δu_{x2} and Δu_{y2} at the crack tip, as given by equations

$$\Delta u_{x2} = \frac{\Delta a}{b}(\Delta u_x) \tag{4}$$

$$\Delta u_{y2} = \frac{\Delta a}{b}(\Delta u_y) \tag{5}$$

where *b* is the horizontal distance between node 1412 and either node 1419 or node 1421. See Figure 6.

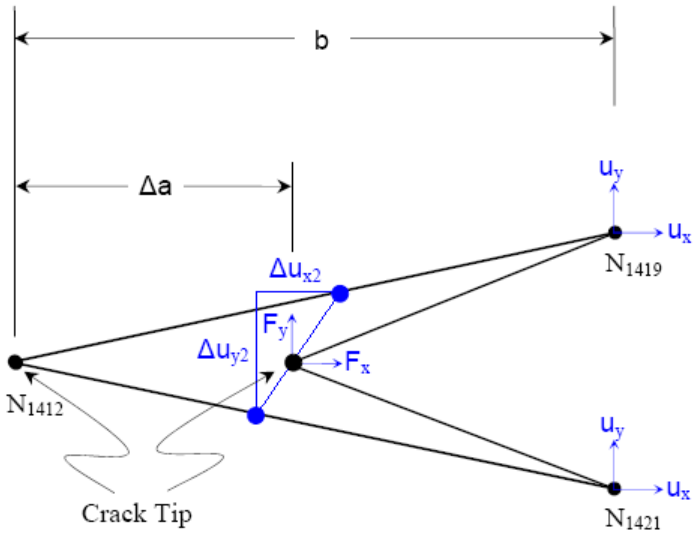

Figure 6. Schematic interpolation of crack tip forces & displacements for fracture mechanics beam model.

4. Energy Release Rate

The energy release rate *G* represents the crack's driving force and is the amount of virtual work associated with opening (or closing) of a crack. *G* is calculated for both mode I and mode II fractures using,

$$G_I = \frac{1}{2} F_y \frac{\Delta u_{y2}}{\Delta a} \tag{6}$$

$$G_{II} = \frac{1}{2} F_x \frac{\Delta u_{x2}}{\Delta a} \tag{7}$$

where for the constrained load at $u_y = 0$ the crack surface is prevented from displacing (i.e., $\Delta u_{y2} = 0$) and thus results in a null energy release rate of $G_I = 0$. Consequently, results from the energy method are presented here only for mode II fractures.

D. FRACTURE MECHANICS PLATE MODEL

The fracture mechanics plate model shows how an edge crack or flaw in the interface of a composite joint propagates under an applied shear load and how this process is influenced by the application of reinforcing particles such as CNTs. These analytical predictions are made by calculating fracture parameters such as energy release rate in the region of a crack in order to estimate crack growth rate. While energy release rate *G* represents the amount of work associated with a crack opening, it is at the point of instability when the change in potential energy equals the change in the crack length that fracture occurs.

1. Composite Plate with Surface Crack

Consider a composite plate with an edge crack as shown in Figure 7. The plate comprises three linear elastic isotropic materials having Young's moduli $E_1 = 50GPa$, $E_2 = 8.0GPa$, $E_3 = 400GPa$ and Poisson's ratios $\nu_1 = 0.30$, $\nu_2 = 0.28$, $\nu_3 = 0.20$. Let length $l = 0.05m$, height $h = 0.05m$, and crack length $a = 0.01m$. The left edge is clamped while the right edge is constrained in the *x* direction and subject to a total applied nodal force $F_y = -5,000N$ to represent distributed shearing load.

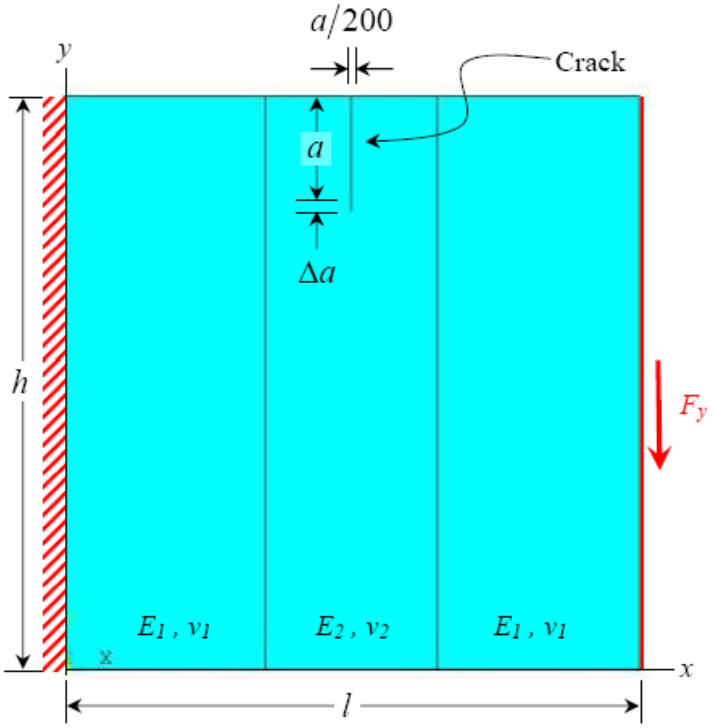

Figure 7. Composite plate with surface crack under applied shear load.

2. FEM Model of Composite Plate with Surface Crack

A two-dimensional FEM model in ANSYS uses higher order eight-node elements (i.e., PLANE82). Each node has two degrees of freedom, u_x and u_y, with the degenerated element having coincident nodes *K*, *L*, and *O* [14].

The crack tip uses quarter-point singular eight-node elements (i.e., PLANE82), where the radius of the first row elements is specified at $a/8 = 1.25mm$ and the second row ratio is set to 50 percent. Linear elastic plane stress behavior is assumed for this static analysis. A very small opening ($\sim a/200$) facilitates modeling of the crack face.

Each area is freely meshed using *smart size* level 1 elements with three refinements. The right side of the plate has applied total force load $F_y = -5kN$ distributed to each node, constrained in the *x* direction. The left side of the plate is clamped and therefore constrained in both *x* and *y* directions. See Figure 8.

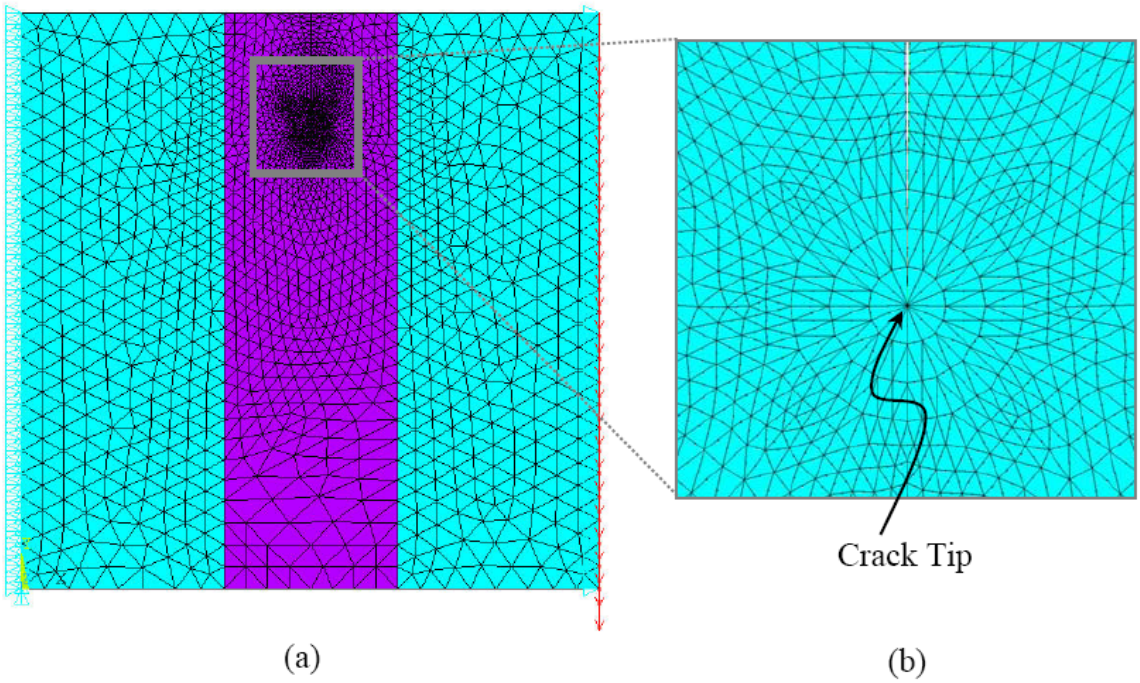

Figure 8. Mesh of fracture mechanics plate model with surface crack (*a*) under shear nodal force with expanded view of crack tip (*b*).

3. Virtual Crack Extension Method

In the virtual crack extension method, two separate analysis are performed, one before extension with crack length a and the other after extension with crack length $a + \Delta a$.

In the first analysis, before extension, a 2-D FEM model obtains the reaction solution for resultant nodal forces F_x and F_y at the crack tip. In this case, the crack tip is located at node 34 and therefore F_x and F_y are taken at that node.

Before starting the second analysis, the crack length is extended. Extension of the crack length is carried out by selecting all nodes in the vicinity of the crack tip, which is defined here as all nodes located within radial distance $r = a/2 = 5mm$ of the crack tip, and then the selected nodes are scaled and moved in the negative y direction for a distance equivalent to 1/2 percent of the crack length. This action results in total crack length extension $\Delta a = 10mm(0.5\%) = 0.05mm$, which corresponds to nodal scaling

factor $R_y = 3.995/4.000$. Crack tip remains at node 34, now at an extended distance from its prior location.

In the second analysis, with crack length extension, a 2-D FEM model obtains the reaction solution for resultant nodal displacement components u_x and u_y at the crack tip. In this case, we take the difference of u_x and u_y between nearest neighboring nodes 41 and 2948 post-solution, using

$$\Delta u_x = u_{x-N41} - u_{x-N2948} \tag{8}$$

$$\Delta u_y = u_{y-N41} - u_{y-N2948} \tag{9}$$

Linear interpolation provides the resultant components of virtual displacement Δu_{x2} and Δu_{y2} at the crack tip, as given by equations

$$\Delta u_{x2} = \frac{\Delta a}{b}\left(\Delta u_x\right) \tag{10}$$

$$\Delta u_{y2} = \frac{\Delta a}{b}\left(\Delta u_y\right) \tag{11}$$

where *b* is the vertical distance between node 34 and either of node 41 or node 2948. See Figure 9.

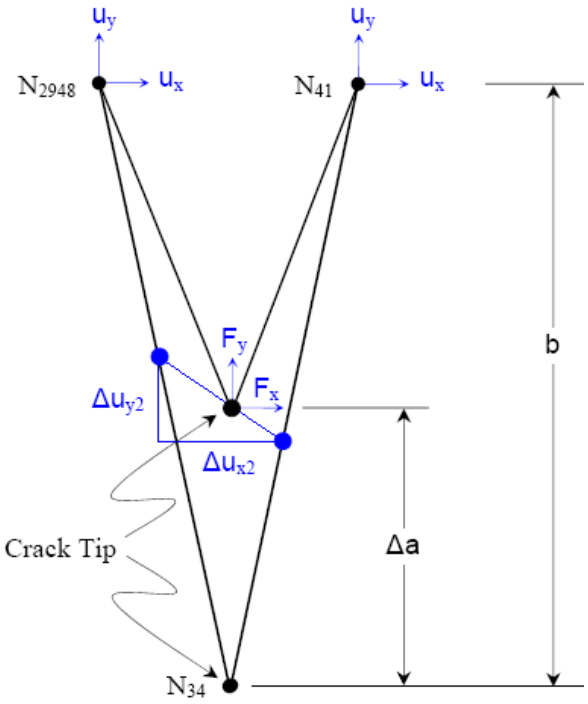

Figure 9. Schematic interpolation of crack tip forces & displacements for fracture mechanics plate model.

4. Energy Release Rate

The energy release rate G represents the crack's driving force and is the amount of virtual work associated with opening (or closing) of a crack. G is calculated for both mode I and mode II fractures using,

$$G_I = \frac{1}{2} F_x \frac{\Delta u_{x2}}{\Delta a} \tag{12}$$

$$G_{II} = \frac{1}{2} F_y \frac{\Delta u_{y2}}{\Delta a} \tag{13}$$

where for the constrained load at $u_x = 0$ the crack surface is prevented from displacing (i.e., $\Delta u_{x2} = 0$) and thus results in a null energy release rate of $G_I = 0$. Consequently, results from the energy method are presented here only for mode II fractures.

THIS PAGE INTENTIONALLY LEFT BLANK

III. RESULTS AND DISCUSSION

A. STRENGTH MODEL

The strength model predicts the effect that reinforcing particles have on the state of stress in the interface of a composite joint. Several types of models are used for comparative analyses, including the homogeneous beam, the baseline composite beam without reinforcing particles, and the composite beam with reinforcing particles where different volume fractions are discretely tested.

1. Homogeneous Beam

Starting with the basic form of a 2-D finite element method (FEM) model, homogeneous beam using base material having Young's modulus $E = 50GPa$ throughout, produces nodal forces and displacements that result in maximum von Mises equivalent stress $\sigma_e = 15.5MPa$. See Table 1.

E_1	u_x	u_y	τ_{max}	σ_{max}	γ_{max}	e_{max}	$\mathcal{U}_{max}$
GPa	*cm*	*cm*	$kg/cm{\cdot}s^2$	$kg/cm{\cdot}s^2$	*cm/cm*	*cm/cm*	$kg \cdot cm^2/s^2$
50.0	1.238E-02	1.520E-04	31,351	154,559	1.63E-04	3.110E-04	7.857E-01

Table 1. Maximum stress and strain of homogeneous beam ($E = 50GPa$).

2. Baseline Composite Beam without Reinforcing Particles

Next, using the baseline 2-D FEM model, composite beam with base and matrix material having Young's moduli $E_1 = 50GPa$ and $E_2 = 8.0GPa$ respectively but without reinforcing particles, produces nodal forces and displacements that result in maximum von Mises equivalent stress $\sigma_e = 11.5MPa$ in the matrix material. See Table 2.

u_x	u_y	τ_{max}	σ_{max}	γ_{max}	e_{max}	$\mathcal{U}_{max}$
cm	*cm*	$kg/cm{\cdot}s^2$	$kg/cm{\cdot}s^2$	*cm/cm*	*cm/cm*	$kg \cdot cm^2/s^2$
1.051E-02	1.587E-03	17,357	114,781	5.550E-04	1.438E-03	6.065E+00

Table 2. Maximum stress and strain in matrix material of baseline composite beam where $E_1 = 50GPa$, $E_2 = 8.0GPa$, without reinforcing particles.

The baseline model results indicate a 24.4% decrease in the maximum von Mises equivalent stress σ_e when compared to the homogeneous model. However, the opposite trend was expected as the relatively softer matrix material now comprises greater than eight percent by volume of the composite beam thus lowering the overall beam stiffness creating a higher state of internal stress.

3. Composite Beam with Reinforcing Particles in Matrix Material

Before modeling reinforcing particles, three different particle sizes *A* are used in two different volume fractions Φ. Small-, medium-, and large-sized particles are used, corresponding to particle size $A = 1.23mm^2$, $A = 4.91mm^2$, and $A = 11.0mm^2$ respectively. The number of particles varies in each model in order to hold constant the volume fraction Φ, which is a function of the number of particles in the matrix material, at either of $\Phi = 7\%$ or $\Phi = 14\%$. See Figure 10. Recall the composite beam is clamped on the left end and has an applied compressive axial force on the right.

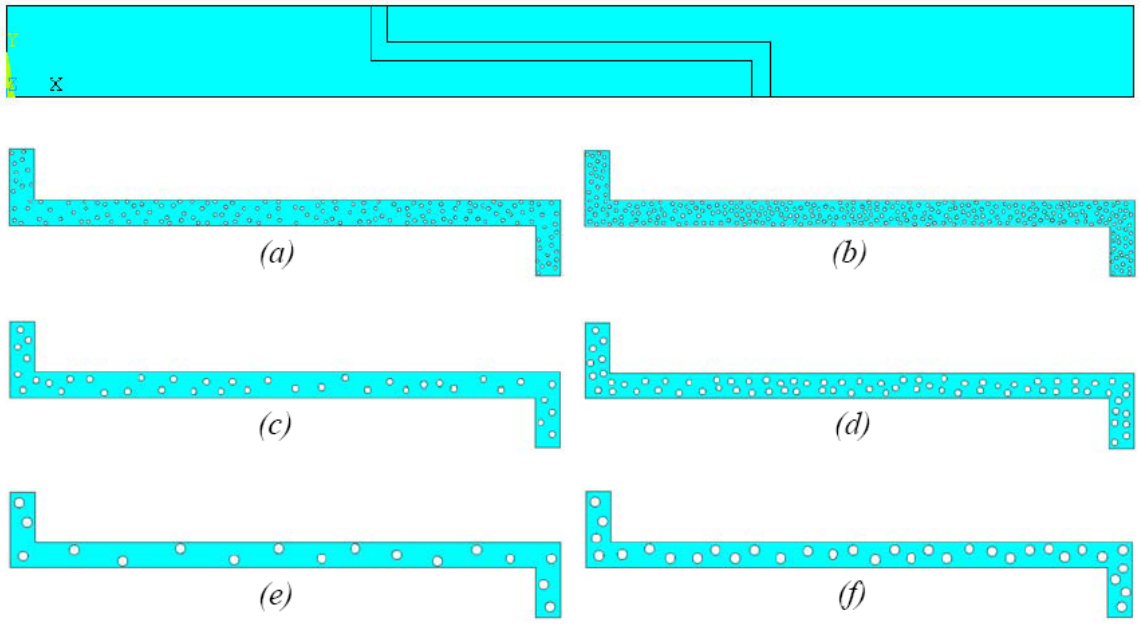

Figure 10. Composite beam matrix material containing reinforcing particles of three sizes A & two volume fractions Φ: $A_{\Phi=7\%} = 1.23mm^2$ (a), $A_{\Phi=14\%} = 1.23mm^2$ (b), $A_{\Phi=7\%} = 4.91mm^2$ (c), $A_{\Phi=14\%} = 4.91mm^2$ (d), $A_{\Phi=7\%} = 11.0mm^2$ (e), $A_{\Phi=14\%} = 11.0mm^2$ (f).

For the varying size model, three distinct simulations are performed, one for each particle size. The lowest number of particles $N_d = 17$ and $N_d = 33$ use the largest size particles $A = 11.0mm^2$ to maintain volume fraction Φ constant. Similarly, the highest number of particles $N_d = 156$ and $N_d = 296$ use the smallest size $A = 1.23mm^2$.

Varying particle size from $A = 1.23mm^2$ to $A = 11.0mm^2$ while holding constant volume fraction Φ at either of $\Phi = 7\%$ or $\Phi = 14\%$ produces nodal forces and displacements that result in maximum von Mises equivalent stress σ_e ranging from $\sigma_e = 16.2MPa$ to $\sigma_e = 20.1MPa$ in the matrix material. See Table 3.

N_d	Φ	u_x	u_y	τ_{max}	σ_{max}	γ_{max}	e_{max}	u_{max}
	%	cm	cm	$kg/cm \cdot s^2$	$kg/cm \cdot s^2$	cm/cm	cm/cm	$kg \cdot cm^2/s^2$
17	7.2%	1.023E-02	1.275E-03	31,863	169,303	1.020E-03	2.133E-03	4.842E+00
33	14.0%	1.012E-02	1.240E-03	44,273	176,270	1.417E-03	2.211E-03	3.596E+00
39	7.4%	1.030E-02	1.386E-03	42,270	162,936	1.353E-03	2.048E-03	2.788E+00
74	14.0%	1.014E-02	1.278E-03	43,881	168,642	1.035E-03	2.141E-03	1.875E+00
156	7.4%	1.031E-02	1.439E-03	48,700	181,902	1.558E-03	3.224E-03	9.574E-01
296	14.0%	1.017E-02	1.309E-03	48,427	200,876	1.550E-03	2.516E-03	5.156E-01

Table 3. Maximum stress and strain in matrix material of composite beam where $E_1 = 50GPa$, $E_2 = 8.0GPa$, $E_3 = 400GPa$, varying particle size from $A = 1.23mm^2$ to $A = 11.0mm^2$ while holding constant volume fraction Φ at either of $\Phi = 7\%$ or $\Phi = 14\%$.

For the varying particle size model, there is an average 49.3% increase in the resultant σ_e for $\Phi = 7\%$ and an average 58.5% increase in the resultant σ_e for $\Phi = 14\%$ when compared to the baseline model. See Table 4.

	σ_e	
Particle Size, mm^2	$\Phi = 7\%$	$\Phi = 14\%$
Small, 1.23	75.0%	58.5%
Medium, 4.91	42.0%	46.9%
Large, 11.0	47.5%	53.6%

Table 4. Average increase in maximum vonMises equivalent stress σ_e varying reinforcing particle size A in matrix material of composite beam when compared to baseline model.

Combined results show the maximum von Mises equivalent stress σ_e initially decreases before rising slightly again as the number of particles decreases with increasing particle size. See Figure 11. The reason for these minima is not fully understood.

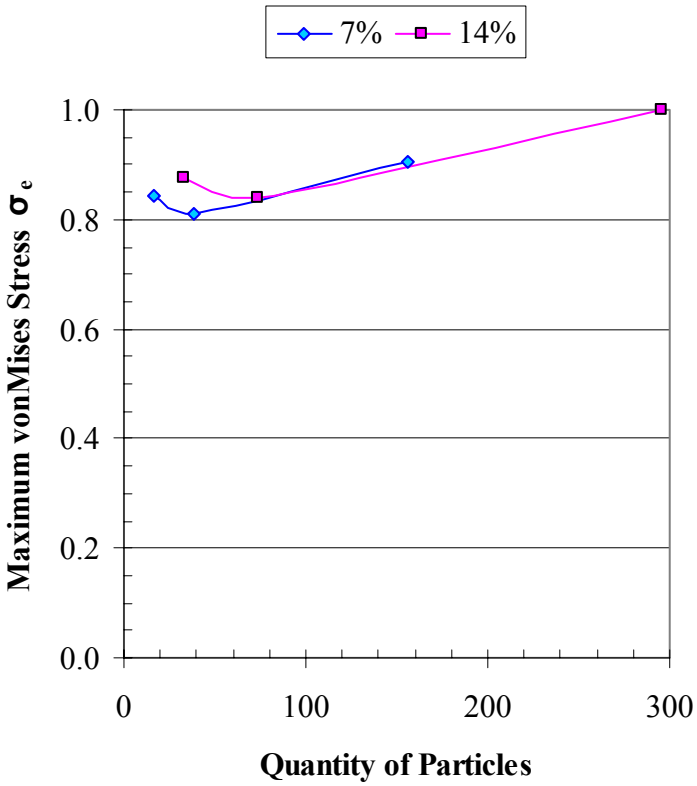

Figure 11. Combined maximum von Mises equivalent stresses σ_e in matrix material of composite beam with reinforcing particles for volume fractions $\Phi = 7\%$ & $\Phi = 14\%$.

The trend here shows a higher volume fraction has a higher maximum von Mises equivalent stress σ_e when compared to the baseline model, with an overlap in stress variances between the maximum and minimum in each model. See Figure 12. However, the opposite trend was expected as the volume fraction goes up the beam is generally stiffer and should reduce the overall state of internal stress.

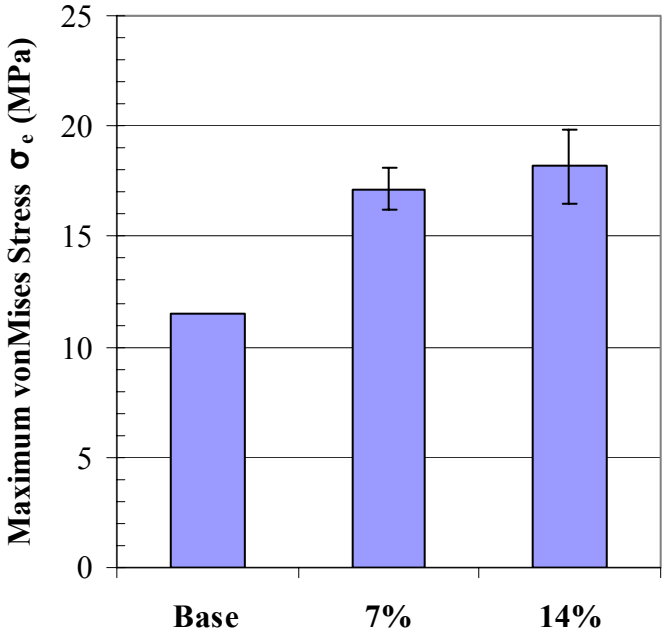

Figure 12. Average maximum von Mises equivalent stress σ_e in matrix material of composite beam with reinforcing particles at volume fraction $\Phi = 7\%$, $\Phi = 14\%$; comparison to base model.

Overall these results suggest the strength model is not a reliable predictor of the failure strength at the interface of a composite beam, thus a different approach is needed.

B. FRACTURE MECHANICS BEAM MODEL

A fracture mechanics based beam model predicts the effect that reinforcing particles have on an internal crack within the interface of a composite joint. Comparative analyses are drawn between the baseline model having no reinforcing particles and a composite beam with reinforcing particles.

1. Baseline Composite Beam without Reinforcing Particles

Jumping right into the baseline 2-D FEM model, composite beam with internal crack but without reinforcing particles, both base and matrix material having Young's

moduli $E_1 = 50GPa$ and $E_2 = 8.0GPa$ respectively, produces nodal forces and displacements at the crack tip that result in energy release rate $G_{II} = 22.6\,mJ/m^2$. See Table 5.

$\mathbf{F_x}$	$\mathbf{u_{x+1}}$	$\mathbf{u_{x-1}}$	$\mathbf{\Delta u_x}$	$\mathbf{\Delta u_{x2}}$	$\mathbf{G_{II}}$
$kg{\cdot}cm/s^2$	cm	cm	cm	cm	J/m^2
-65.03	-9.5869E-03	-9.5654E-03	-2.1500E-05	-3.4677E-06	2.2550E-02

Table 5. Energy release rate G_{II} in matrix material of baseline composite beam where $E_1 = 50GPa$, $E_2 = 8.0GPa$.

2. Composite Beam with Reinforcing Particles in Matrix Material

Next, application of reinforcing particles having Young's modulus $E_3 = 400GPa$ to the matrix material containing an internal crack, produces nodal forces and displacements at the crack tip that result in energy release rate $G_{II} = 22.2\,mJ/m^2$. See Table 6.

$\mathbf{F_x}$	$\mathbf{u_{x+1}}$	$\mathbf{u_{x-1}}$	$\mathbf{\Delta u_x}$	$\mathbf{\Delta u_{x2}}$	$\mathbf{G_{II}}$
$kg{\cdot}cm/s^2$	cm	cm	cm	cm	J/m^2
-61.73	-9.4534E-03	-9.4354E-03	-1.8000E-05	-3.6000E-06	2.2222E-02

Table 6. Energy release rate G_{II} in matrix material of composite beam with reinforcing particles where $E_3 = 400GPa$.

Results from composite beam with reinforcing particles indicate 1.5% reduction in rate of energy release G_{II} when compared to the baseline model. This trend is encouraging and suggests the fracture mechanics beam model is a reliable predictor of energy release rates for a composite beam with internal crack at the interface.

Now that this methodology has been validated, a more detailed fracture mechanics model is needed in order to predict how reinforcing particles affect interface strength.

C. FRACTURE MECHANICS PLATE MODEL

A fracture mechanics based plate model predicts the effect that reinforcing particles have on a surface crack within the interface of a composite joint. Several types of models are used for comparative analyses, including the homogeneous plate, the baseline plate without reinforcing particles, and composite plates with reinforcing particles where the size, stiffness, and quantity of reinforcing particles are discretely tested.

1. Homogeneous Plate

Starting with a basic form of 2-D FEM model, the homogeneous plate using base material having Young's modulus $E = 50GPa$ throughout, produces nodal forces and displacements at the crack tip that result in energy release rate $G_{II} = 8.39\, J/m^2$. See Table 7.

$\mathbf{F_y}$	$\mathbf{u_{y+1}}$	$\mathbf{u_{y-1}}$	$\mathbf{\Delta u_y}$	$\mathbf{\Delta u_{y2}}$	$\mathbf{G_{II}}$
$kg \cdot cm/s^2$	cm	cm	cm	cm	J/m^2
-3179.4	-2.0333E-03	-1.9510E-03	-8.2300E-05	-2.6378E-05	8.3867E+00

Table 7. Energy release rate G_{II} in homogeneous plate ($E = 50GPa$).

2. Baseline Composite Plate without Reinforcing Particles

Next, the baseline 2-D FEM model, composite plate with both base and matrix material having Young's moduli $E_1 = 50GPa$ and $E_2 = 8.0GPa$ respectively but without reinforcing particles, produces nodal forces and displacements at the crack tip that result in energy release rate $G_{II} = 67.4\, J/m^2$. See Table 8.

$\mathbf{F_y}$	$\mathbf{u_{y+1}}$	$\mathbf{u_{y-1}}$	$\mathbf{\Delta u_y}$	$\mathbf{\Delta u_{y2}}$	$\mathbf{G_{II}}$
$kg \cdot cm/s^2$	cm	cm	cm	cm	J/m^2
-3606.9	-4.7695E-03	-4.1865E-03	-5.8300E-04	-1.8686E-04	6.7398E+01

Table 8. Energy release rate G_{II} in matrix material of baseline composite plate where $E_1 = 50GPa$, $E_2 = 8.0GPa$ without reinforcing particles.

The baseline model results indicate a substantial seven-fold increase in rate of energy release G_{II} when compared to the homogeneous model. This trend is expected as the relatively softer matrix material now comprises about one third of the composite plate surrounding the crack tip thus facilitating crack propagation and causing G_{II} to increase nearly one order of magnitude.

3. Composite Plate with Reinforcing Particles in Matrix Material

Before modeling reinforcing particles, test positions are established in the matrix material relative to the crack tip. Particle positions *a*, *b*, and *c*, are located radial distance *r* from the crack tip in the negative *x*, negative *y*, and positive *x* directions respectively. See Figure 13. Recall the composite plate is clamped on the left end and has a transverse nodal shearing force on the right.

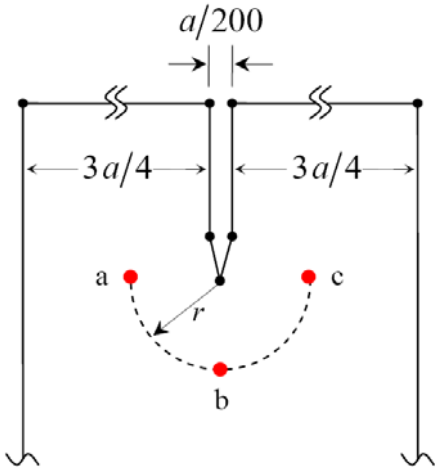

Figure 13. Composite plate matrix material containing reinforcing particles *a*, *b*, *c* in position radial distance *r* to crack tip.

4. Composite Plate with Varying Particle Position

For the varying particle position model, three distinct simulations are performed, one for each particle position, followed by one additional simulation for all three particles together.

a. ***Particle at Position* a**

Varying particle *a* stiffness from $E_3 = 8.0GPa$ to $E_3 = 500GPa$ while holding constant particle size $A = 0.03961mm^2$ at distance $r = 1.124mm$ to crack tip produces nodal forces and displacements at the crack tip that result in energy release rates ranging from $G_{II} = 67.4\,J/m^2$ down to $G_{II} = 67.3\,J/m^2$. See Table 9.

E_3	F_y	u_{y+1}	u_{y-1}	Δu_y	Δu_{y2}	G_{II}
GPa	*kg·cm/s²*	*cm*	*cm*	*cm*	*cm*	*J/m²*
8.0	-3,607.2	-4.7695E-03	-4.1865E-03	-5.8300E-04	-1.8686E-04	6.7404E+01
20	-3,606.1	-4.7691E-03	-4.1864E-03	-5.8270E-04	-1.8676E-04	6.7349E+01
50	-3,605.2	-4.7689E-03	-4.1864E-03	-5.8250E-04	-1.8670E-04	6.7309E+01
80	-3,605.0	-4.7688E-03	-4.1864E-03	-5.8240E-04	-1.8667E-04	6.7293E+01
140	-3,604.8	-4.7688E-03	-4.1864E-03	-5.8240E-04	-1.8667E-04	6.7290E+01
200	-3,604.7	-4.7688E-03	-4.1864E-03	-5.8240E-04	-1.8667E-04	6.7288E+01
250	-3,604.6	-4.7688E-03	-4.1864E-03	-5.8240E-04	-1.8667E-04	6.7286E+01
300	-3,604.6	-4.7687E-03	-4.1864E-03	-5.8230E-04	-1.8663E-04	6.7274E+01
400	-3,604.5	-4.7687E-03	-4.1864E-03	-5.8230E-04	-1.8663E-04	6.7272E+01
500	-3,604.5	-4.7687E-03	-4.1864E-03	-5.8230E-04	-1.8663E-04	6.7272E+01

Table 9. Energy release rate G_{II} for reinforcing particle *a* in matrix material of composite plate varying particle stiffness from $E_3 = 8.0GPa$ to $E_3 = 500GPa$ with particle size $A = 0.03961mm^2$ at distance $r = 1.124mm$ to crack tip.

b. ***Particle at Position* b**

Varying particle *b* stiffness from $E_3 = 8.0GPa$ to $E_3 = 500GPa$ while holding constant particle size $A = 0.03961mm^2$ at distance $r = 1.124mm$ to crack tip produces nodal forces and displacements at the crack tip that result in energy release rates ranging from $G_{II} = 67.4\,J/m^2$ down to $G_{II} = 66.8\,J/m^2$. See Table 10.

E_3	F_y	u_{y+1}	u_{y-1}	Δu_y	Δu_{y2}	G_{II}
GPa	*kg·cm/s²*	*cm*	*cm*	*cm*	*cm*	*J/m²*
8.0	-3,606.3	-4.7694E-03	-4.1865E-03	-5.8290E-04	-1.8683E-04	6.7375E+01
20	-3,598.8	-4.7685E-03	-4.1868E-03	-5.8170E-04	-1.8644E-04	6.7097E+01
50	-3,594.5	-4.7680E-03	-4.1869E-03	-5.8110E-04	-1.8625E-04	6.6948E+01
80	-3,593.2	-4.7678E-03	-4.1869E-03	-5.8090E-04	-1.8619E-04	6.6900E+01
140	-3,592.1	-4.7677E-03	-4.1870E-03	-5.8070E-04	-1.8612E-04	6.6857E+01
200	-3,591.7	-4.7677E-03	-4.1870E-03	-5.8070E-04	-1.8612E-04	6.6849E+01
250	-3,591.5	-4.7676E-03	-4.1870E-03	-5.8060E-04	-1.8609E-04	6.6834E+01
300	-3,591.3	-4.7676E-03	-4.1870E-03	-5.8060E-04	-1.8609E-04	6.6830E+01
400	-3,591.1	-4.7676E-03	-4.1870E-03	-5.8060E-04	-1.8609E-04	6.6827E+01
500	-3,591.0	-4.7676E-03	-4.1870E-03	-5.8060E-04	-1.8609E-04	6.6825E+01

Table 10. Energy release rate G_{II} for reinforcing particle *b* in matrix material of composite plate varying particle stiffness from $E_3 = 8.0GPa$ to $E_3 = 500GPa$ with particle size $A = 0.03961mm^2$ at distance $r = 1.124mm$ to crack tip.

c. Particle at Position c

Varying particle *c* stiffness from $E_3 = 8.0GPa$ to $E_3 = 500GPa$ while holding constant particle size $A = 0.03961mm^2$ at distance $r = 1.124mm$ to crack tip produces nodal forces and displacements at the crack tip that result in energy release rates ranging from $G_{II} = 67.4\,J/m^2$ down to $G_{II} = 67.2\,J/m^2$. See Table 11.

E_3	F_y	u_{y+1}	u_{y-1}	Δu_y	Δu_{y2}	G_{II}
GPa	$kg{\cdot}cm/s^2$	*cm*	*cm*	*cm*	*cm*	J/m^2
8.0	-3,607.1	-4.7695E-03	-4.1865E-03	-5.8300E-04	-1.8686E-04	6.7402E+01
20	-3,603.4	-4.7693E-03	-4.1866E-03	-5.8270E-04	-1.8676E-04	6.7298E+01
50	-3,601.0	-4.7691E-03	-4.1866E-03	-5.8250E-04	-1.8670E-04	6.7230E+01
80	-3,600.3	-4.7691E-03	-4.1867E-03	-5.8240E-04	-1.8667E-04	6.7206E+01
140	-3,599.8	-4.7690E-03	-4.1867E-03	-5.8230E-04	-1.8663E-04	6.7185E+01
200	-3,599.5	-4.7690E-03	-4.1867E-03	-5.8230E-04	-1.8663E-04	6.7179E+01
250	-3,599.4	-4.7690E-03	-4.1867E-03	-5.8230E-04	-1.8663E-04	6.7177E+01
300	-3,599.3	-4.7690E-03	-4.1867E-03	-5.8230E-04	-1.8663E-04	6.7175E+01
400	-3,599.2	-4.7690E-03	-4.1867E-03	-5.8230E-04	-1.8663E-04	6.7174E+01
500	-3,599.2	-4.7690E-03	-4.1867E-03	-5.8230E-04	-1.8663E-04	6.7174E+01

Table 11. Energy release rate G_{II} for reinforcing particle *c* in matrix material of composite plate varying particle stiffness from $E_3 = 8.0GPa$ to $E_3 = 500GPa$ with particle size $A = 0.03961mm^2$ at distance $r = 1.124mm$ to crack tip.

d. Particles at Positions a, b, c

Varying combined particles *abc* stiffness from $E_3 = 8.0GPa$ to $E_3 = 500GPa$ while holding constant particle size $A = 0.03961mm^2$ at distance $r = 1.124mm$ to crack tip produces nodal forces and displacements at the crack tip that result in energy release rates ranging from $G_{II} = 67.4\,J/m^2$ down to $G_{II} = 66.5\,J/m^2$. See Table 12.

E_3	F_y	u_{y+1}	u_{y-1}	Δu_y	Δu_{y2}	G_{II}
GPa	$kg{\cdot}cm/s^2$	*cm*	*cm*	*cm*	*cm*	J/m^2
8.0	-3606.8	-4.7695E-03	-4.1865E-03	-5.8300E-04	-1.8686E-04	6.7396E+01
20	-3594.3	-4.7679E-03	-4.1868E-03	-5.8110E-04	-1.8625E-04	6.6944E+01
50	-3586.8	-4.7670E-03	-4.1870E-03	-5.8000E-04	-1.8590E-04	6.6678E+01
80	-3584.5	-4.7668E-03	-4.1870E-03	-5.7980E-04	-1.8583E-04	6.6612E+01
140	-3582.6	-4.7665E-03	-4.1871E-03	-5.7940E-04	-1.8571E-04	6.6531E+01
200	-3581.8	-4.7664E-03	-4.1871E-03	-5.7930E-04	-1.8567E-04	6.6504E+01
250	-3581.4	-4.7664E-03	-4.1871E-03	-5.7930E-04	-1.8567E-04	6.6497E+01
300	-3581.2	-4.7664E-03	-4.1871E-03	-5.7930E-04	-1.8567E-04	6.6493E+01
400	-3580.9	-4.7663E-03	-4.1871E-03	-5.7920E-04	-1.8564E-04	6.6476E+01
500	-3580.6	-4.7663E-03	-4.1871E-03	-5.7920E-04	-1.8564E-04	6.6471E+01

Table 12. Energy release rate G_{II} for reinforcing particle *abc* in matrix material of composite plate varying particle stiffness from $E_3 = 8.0GPa$ to $E_3 = 500GPa$ with particle size $A = 0.03961mm^2$ at distance $r = 1.124mm$ to crack tip.

For the discrete varying particle stiffness models, there is an average 0.4% decrease in the resultant energy release rate G_{II} when compared to the baseline model. This average increases to 1.2% when all three positions are combined. See Table 13. Individual results at $E_3 = 8.0GPa$ for each varying stiffness model demonstrate continuity with the baseline model.

Particle Location	G_{II}
a	−0.2%
b	−0.8%
c	−0.3%
abc	−1.2%

Table 13. Average decrease in energy release rate G_{II} for reinforcing particles *a,b,c*, when compared to baseline model.

Combined results show energy release rate G_{II} decreases as particle stiffness increases when compared to the baseline model. See Figure 14. In addition, G_{II} asymptotically tends to zero for elastic modulus above $E_3 = 200GPa$

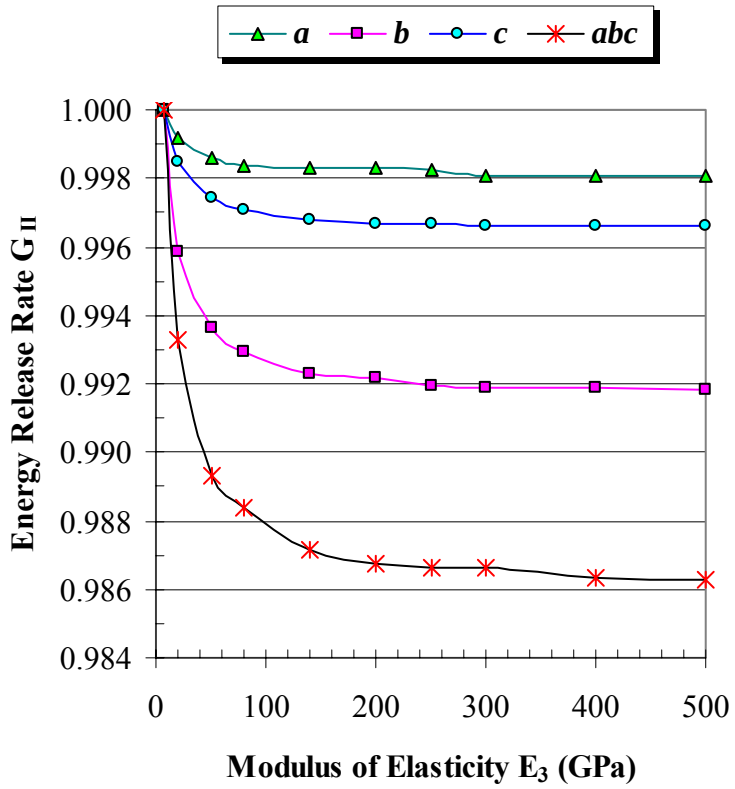

Figure 14. Combined energy release rates G_{II} for reinforcing particles *a*, *b*, *c*, in matrix material of composite plate varying particle stiffness from $E_3 = 8.0GPa$ to $E_3 = 500GPa$ with particle size $A = 0.03961mm^2$ at distance $r = 1.124mm$ to crack tip.

The trend here shows that while particle *b* has the largest single decrease in G_{II}, a more favorable decrease is predicted when all three positions *a*, *b*, and *c*, are combined. See Figure 15. These results are expected as particle *b* is positioned favorably to have greatest influence over the amount of energy released in mode II fractures of this kind.

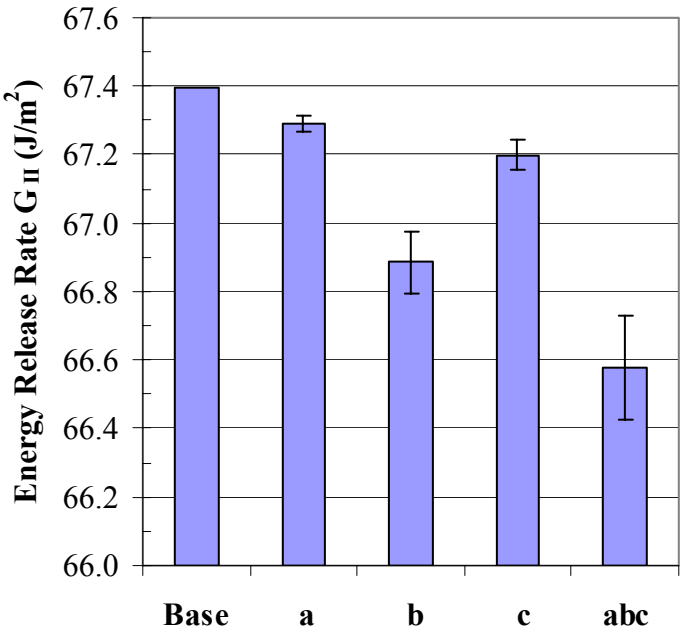

Figure 15. Average energy release rate G_{II} for reinforcing particles *a*, *b*, *c*, in matrix material varying particle stiffness from $E_3 = 8.0GPa$ to $E_3 = 500GPa$ with particle size $A = 0.03961mm^2$ at distance $r = 1.124mm$ to crack tip; comparison to baseline model.

5. Composite Plate with Varying Particle *b* Distance to Crack Tip

Building on prior results, particle *b* is again selected in varying distances to the crack tip. In this case, varying particle *b* distance *r* to crack tip from $r = 0$ to $r = 2.937mm$ while holding constant particle stiffness $E_3 = 400GPa$ produces nodal forces and displacements at the crack tip that result in energy release rates ranging from $G_{II} = 62.5\,J/m^2$ up to $G_{II} = 67.3\,J/m^2$. See Table 14.

r	$\mathbf{F_y}$	$\mathbf{u_{y+1}}$	$\mathbf{u_{y-1}}$	$\mathbf{\Delta u_y}$	$\mathbf{\Delta u_{y2}}$	$\mathbf{G_{II}}$
cm	$kg{\cdot}cm/s^2$	*cm*	*cm*	*cm*	*cm*	J/m^2
0.0000	-3481.9	-4.7556E-03	-4.1957E-03	-5.5990E-04	-1.7946E-04	6.2484E+01
0.0312	-3537.5	-4.7630E-03	-4.1902E-03	-5.7280E-04	-1.8359E-04	6.4945E+01
0.0625	-3574.7	-4.7661E-03	-4.1879E-03	-5.7820E-04	-1.8532E-04	6.6247E+01
0.0938	-3591.2	-4.7676E-03	-4.1870E-03	-5.8060E-04	-1.8609E-04	6.6829E+01
0.1124	-3591.1	-4.7676E-03	-4.1870E-03	-5.8060E-04	-1.8609E-04	6.6827E+01
0.1428	-3592.1	-4.7675E-03	-4.1868E-03	-5.8070E-04	-1.8612E-04	6.6857E+01
0.1625	-3597.4	-4.7682E-03	-4.1867E-03	-5.8150E-04	-1.8638E-04	6.7048E+01
0.1857	-3602.1	-4.7686E-03	-4.1864E-03	-5.8220E-04	-1.8660E-04	6.7216E+01
0.2383	-3603.5	-4.7687E-03	-4.1863E-03	-5.8240E-04	-1.8667E-04	6.7265E+01
0.2937	-3603.6	-4.7687E-03	-4.1862E-03	-5.8250E-04	-1.8670E-04	6.7279E+01

Table 14. Energy release rate G_{II} for reinforcing particle *b* in matrix material of composite plate varying distance r to crack tip from $r = 0$ to $r = 2.937mm$ with particle stiffness $E_3 = 400GPa$.

For the varying particle *b* distance model, there is an average 1.6% decrease in the resultant energy release rate G_{II} when compared to the prior baseline models. See Table 15. In addition, individual results from $r = 1.124mm$ demonstrate continuity with the prior stiffness model.

Distance to Crack Tip, mm	$\boldsymbol{G_{II}}$
0	−7.3%
0.3	−3.6%
0.6	−1.7%
0.9	−0.9%
1.1	−0.9%
1.4	−0.8%
1.6	−0.5%
1.9	−0.3%
2.4	−0.2%
2.9	−0.2%

Table 15. Average decrease in energy release rate G_{II} for particle *b* varying distance *r* to crack tip when compared to baseline model.

Combined results show energy release rate G_{II} decreases as particle *b* distance to the crack tip decreases (i.e., closest to the crack tip). See Figure 16. In addition, G_{II} asymptotically tends to zero at distances greater than $r = 2mm$, providing a clear line of demarcation where reinforcing particles no longer influence crack propagation.

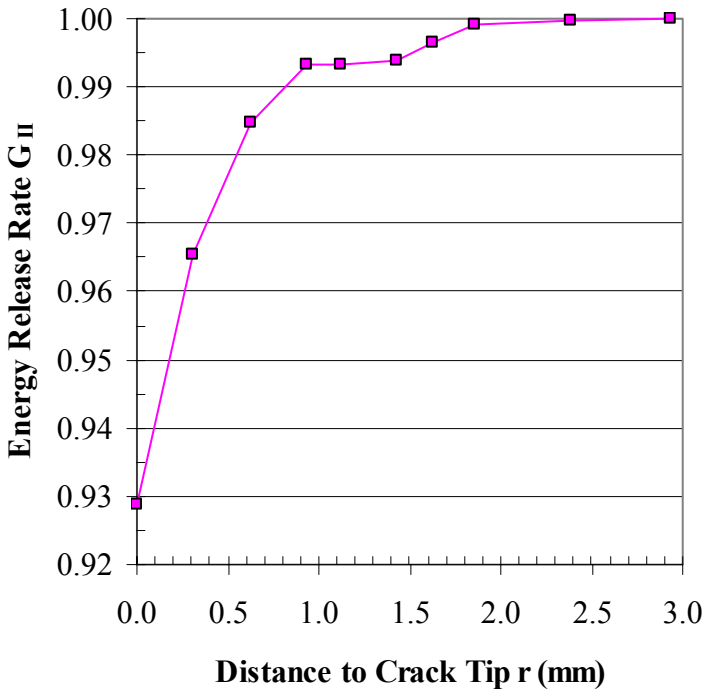

Figure 16. Energy release rate G_{II} for reinforcing particle *b* in matrix material of composite plate varying distance *r* to crack tip from $r = 0$ to $r = 3mm$ with particle stiffness $E_3 = 400GPa$.

6. Composite Plate with Varying Particle Size at Prescribed Distance to Crack Tip

Particle *b* is again used for varying particle size at prescribed distance *r* to crack tip. In this case, varying particle *b* size from $A = 0.01mm^2$ to $A = 2mm^2$ while holding constant particle stiffness $E_3 = 400GPa$ at $r = 1.124mm$ to crack tip produces nodal forces and displacements at the crack tip that result in energy release rates ranging from $G_{II} = 67.2\,J/m^2$ down to $G_{II} = 53.6\,J/m^2$. See Table 16.

A	$\mathbf{F_y}$	$\mathbf{u_{y+1}}$	$\mathbf{u_{y-1}}$	$\mathbf{\Delta u_y}$	$\mathbf{\Delta u_{y2}}$	$\mathbf{G_{II}}$
mm^2	$kg{\cdot}cm/s^2$	*cm*	*cm*	*cm*	*cm*	J/m^2
0.01	-3602.2	-4.7689E-03	-4.1866E-03	-5.8230E-04	-1.8663E-04	6.7230E+01
0.04	-3591.1	-4.7676E-03	-4.1870E-03	-5.8060E-04	-1.8609E-04	6.6827E+01
0.15	-3548.8	-4.7625E-03	-4.1884E-03	-5.7410E-04	-1.8401E-04	6.5300E+01
0.36	-3481.6	-4.7538E-03	-4.1901E-03	-5.6370E-04	-1.8067E-04	6.2903E+01
0.70	-3390.1	-4.7409E-03	-4.1914E-03	-5.4950E-04	-1.7612E-04	5.9707E+01
1.17	-3298.4	-4.7264E-03	-4.1914E-03	-5.3500E-04	-1.7147E-04	5.6559E+01
1.82	-3210.7	-4.7103E-03	-4.1893E-03	-5.2100E-04	-1.6699E-04	5.3615E+01

Table 16. Energy release rate G_{II} for reinforcing particle *b* in matrix material of composite plate varying particle size from $A = 0.01mm^2$ to $A = 2mm^2$ with particle stiffness $E_3 = 400GPa$ at prescribed distance $r = 1.124mm$ to crack tip.

For the varying particle size model, there is an average 8.4% decrease in the resultant energy release rate G_{II} when compared to the prior baseline model. See Table 17. In addition, individual results from $A = 0.04mm^2$ demonstrate continuity with the prior distance model.

Particle Size, mm²	G_{II}
0.01	−0.3%
0.04	−0.8%
0.15	−3.1%
0.36	−6.7%
0.70	−11%
1.2	−16%
1.8	−21%

Table 17. Average decrease in energy release rate G_{II} for particle *b* while varying size *A* when compared to baseline model.

Combined results show energy release rate G_{II} monotonically decreases as particle *b* size increases. See Figure 17.

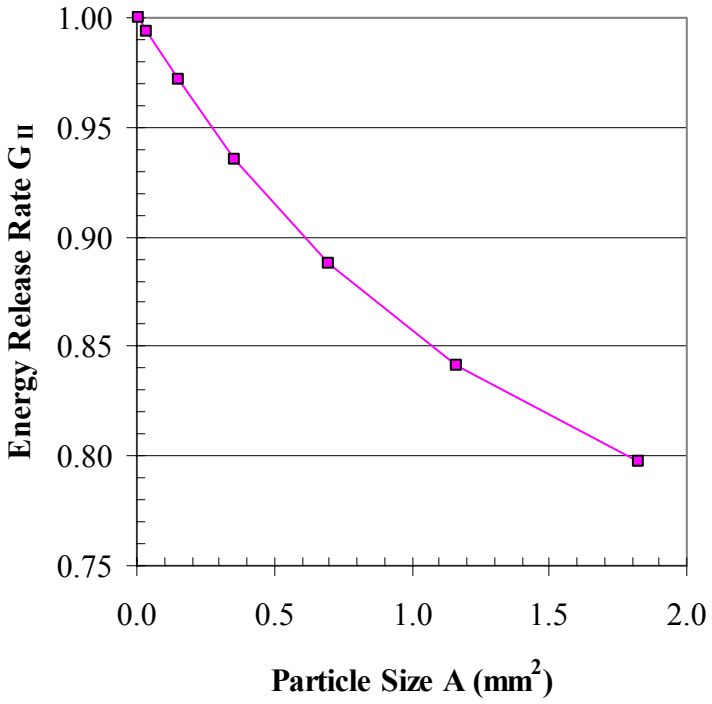

Figure 17. Energy release rate G_{II} for reinforcing particle *b* in matrix material of composite plate varying particle size from $A = 0.01mm^2$ to $A = 2mm^2$ with particle stiffness $E_3 = 400GPa$ at prescribed distance $r = 1.124mm$ to crack tip.

7. Composite Plate with Varying Particle Stiffness Nearest Crack Tip

Next, particle *b* is located near the crack tip at distance $r = 0.3mm$ and under varying particle stiffness from $E_3 = 8.0GPa$ to $E_3 = 500GPa$ produces nodal forces and displacements at the crack tip that result in energy release rates ranging from $G_{II} = 67.3\,J/m^2$ down to $G_{II} = 64.9\,J/m^2$. See Table 18.

E_3	F_y	u_{y+1}	u_{y-1}	Δu_y	Δu_{y2}	G_{II}
GPa	$kg \cdot cm/s^2$	*cm*	*cm*	*cm*	*cm*	J/m^2
8.0	-3604.0	-4.7692E-03	-4.1867E-03	-5.8250E-04	-1.8670E-04	6.7286E+01
20	-3571.3	-4.7662E-03	-4.1884E-03	-5.7780E-04	-1.8519E-04	6.6138E+01
50	-3553.0	-4.7645E-03	-4.1894E-03	-5.7510E-04	-1.8433E-04	6.5491E+01
80	-3547.3	-4.7640E-03	-4.1897E-03	-5.7430E-04	-1.8407E-04	6.5295E+01
140	-3542.5	-4.7635E-03	-4.1899E-03	-5.7360E-04	-1.8385E-04	6.5127E+01
200	-3540.4	-4.7633E-03	-4.1900E-03	-5.7330E-04	-1.8375E-04	6.5055E+01
250	-3539.3	-4.7632E-03	-4.1901E-03	-5.7310E-04	-1.8369E-04	6.5012E+01
300	-3538.5	-4.7631E-03	-4.1901E-03	-5.7300E-04	-1.8365E-04	6.4986E+01
400	-3537.5	-4.7630E-03	-4.1902E-03	-5.7280E-04	-1.8359E-04	6.4945E+01
500	-3536.9	-4.7629E-03	-4.1902E-03	-5.7270E-04	-1.8356E-04	6.4923E+01

Table 18. Energy release rate G_{II} for reinforcing particle *b* in matrix material of composite plate varying particle stiffness from $E_3 = 8.0GPa$ to $E_3 = 500GPa$ with particle located nearest the crack tip at distance $r = 0.3mm$.

Results from varying particle stiffness nearest the crack tip show there is an average 2.9% decrease in the resultant energy release rate G_{II} when compared to the prior baseline model. See Table 19. In addition, individual results from $E_3 = 8.0GPa$ demonstrates continuity with the baseline model.

Particle Stiffness	G_{II}
1.0	−0.2%
2.5	−1.9%
6.3	−2.8%
10.0	−3.1%
17.5	−3.4%
25.0	−3.5%
31.3	−3.5%
37.5	−3.6%
50.0	−3.6%
62.5	−3.7%

Table 19. Average decrease in energy release rate G_{II} for particle *b* while varying stiffness E_3 when compared to baseline model.

Combined results show energy release rate G_{II} decreases as particle *b* stiffness increases. See Figure 18.

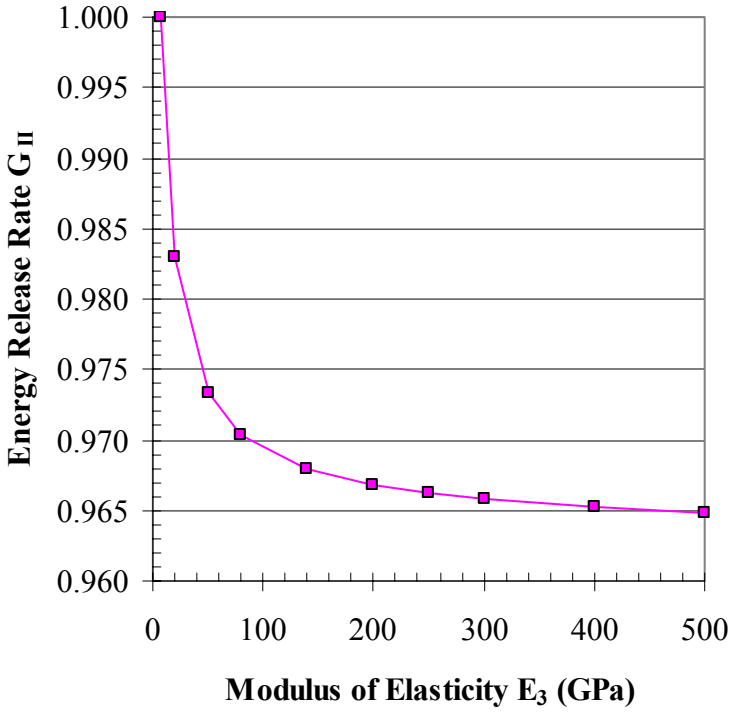

Figure 18. Energy release rate G_{II} for reinforcing particle *b* in matrix material of composite plate varying particle stiffness from $E_3 = 8.0GPa$ to $E_3 = 500GPa$ with particle located nearest the crack tip at $r = 0.3mm$.

THIS PAGE INTENTIONALLY LEFT BLANK

IV. CONCLUSIONS AND RECOMMENDATIONS

A. CONCLUSIONS

Two-dimensional continuum modeling reliably and efficiently predict how the size, quantity, and stiffness of reinforcing particles such as carbon nanotubes (CNTs) affect failure mechanisms at the interface of composite structures, depending on which methodology is used.

The strength model revealed that adding reinforcing particles to the matrix material of a scarf joint causes the maximum von Mises equivalent stress to increase. This result was contrary to what had been expected. Adding reinforcing particles to the interface of the composites should have increased the interface strength. Therefore, based on these results, the strength model does not reliably predict the effect that reinforcing particles have on state of stress in the interface of a composite joint.

The fracture mechanics based beam model illustrated that application of reinforcing particles to the matrix material of a composite beam with an internal crack causes the energy release rate to favorably decrease approximately two percent. This result was encouraging and served as the basis for validation of the methodology to proceed with a more detailed fracture mechanics model of the interface.

The fracture mechanics plate model revealed many aspects of particle reinforcement in a composite joint. First, application of three reinforcing particles near the crack tip favorably reduces the energy release rate one percent on average. When presented discretely the magnitudes of one particle were greater than the others, thus energy release rate is a strong function of particle position relative to the crack tip. Second, a single reinforcing particle located at the crack tip favorably reduces the energy release rate seven percent on average, thus energy release rate is a strong function of reinforcing particle distance to the crack tip. Third, energy release rate monotonically decreases as the reinforcing particle size increases. Finally, application of reinforcing particles that are ten times stiffer than the surrounding matrix material favorably reduces

the energy release rate by 3 percent on average. Therefore, based on these combined results, the fracture mechanics plate model appears to reliably predict the effect that reinforcing particles have on energy release rate in the interface of a composite plate with surface crack. Additionally, model setup time is estimated to be approximately one hour with solution time of less than one minute for each iteration. Moreover, model storage requirements are nominal with file size of approximately 12MB, which includes all pre-processing and meshing. Therefore, in addition to being reliable, the model is also highly efficient in terms of time and space.

B. RECOMMENDATIONS

Continuum modeling of interface failure represents reliable and efficient modeling of composite interfaces designed to improve their failure strength through the addition of nanoscale reinforcing particles such as carbon nanotubes (CNTs). This type of modeling is a useful tool to predict and improve the failure strength of composite structures. The model can be used to help focus future research in the structural applications of CNTs, especially within testing and evaluation of CNTs in composite scarf joint interfaces. In addition, atomic level modeling is recommended for the interface failure to be compared with the continuum models. The atomic model can include nanoparticles such as CNTs as well as the polymer matrix as they are without smearing. Additionally, multi-scale modeling will be beneficial to include different length-scale characteristics in the design and analysis of composite joints containing nanoparticles.

LIST OF REFERENCES

[1] S. Iijima, "Helical microtubules of graphitic carbon," *Nature*, vol. 354, pp. 56-58, Nov. 1991.

[2] M.M.J. Treacy, T.W. Ebbesen, J.M. Gibson, "Exceptionally high Young's modulus observed for individual carbon nanotubes," *Nature*, vol. 381, pp. 678-680, June 1996.

[3] A. Krishnan, E. Dujardin, T.W. Ebbesen, P.N. Yianilos, M.M.J. Treacy, "Young's modulus of single-walled nanotubes," *Physical Review* B, vol. 58, no. 20, p.14013-14019, Nov. 1998.

[4] B.I. Yakobson, C.J. Brabec, J. Bernholc, "Nanomechanics of carbon tubes: Instabilities beyond linear response," *Physical Review Letters*, vol. 76, no. 14, pp. 2511-2514, April 1996.

[5] S. Iijima, C. Brabec, A. Maiti, J. Bernholc, "Structural flexibility of carbon nanotubes," *Journal of Chemical Physics*, vol. 104, no. 5, pp. 2089-2092, Feb. 1996.

[6] J.J. Oh, "Determination of Young's modulus of carbon nanotubes using MD simulation," M.S. thesis, Naval Postgraduate School, Monterey, CA, 2003.

[7] V.N. Popov, V.E. Van Doren, M. Balkanski, "Elastic properties of single-walled carbon nanotubes," *Physical Review* B, vol. 61, no. 4, pp. 3078-3084, Jan. 2000.

[8] G.M. Odegard, T.S. Gates, L.M. Nicholson, K.E. Wise, "Equivalent-continuum modeling with application to carbon nanotube," *Composites Science and Technology*, vol. 62, no. 14, pp.1869-1880, Nov. 2002.

[9] R.S. Rouff, D. Qian, W.K. Liu, "Mechanical properties of carbon nanotubes: Theoretical predictions and experimental measurements," *Comptes Rendus Physique*, vol. 4, pp. 993-1008, 2003.

[10] D. Qian, E.C. Dickey, R. Andrews, T. Rantell, "Load transfer and deformation mechanisms in carbon nanotube-polystyrene composites," *Applied Physics Letters*, vol. 76, no. 20, pp. 2868-2870, May 2000.

[11] O. Lourie, D.M. Cox, H.D. Wagner, "Buckling and collapse of embedded carbon nanotubes," *Physical Review Letters*, vol. 81, no. 8, pp. 1638-1641, Aug. 1998.

[12] R.E. Slaff, Jr., "The enhancement of composite scarf joint interface strength through carbon nanotubes reinforcement," M.S. thesis, Naval Postgraduate School, Monterey, CA, 2007.

[13] A.C. Ugural and S.K. Fenster, *Advanced Strength and Applied Elasticity*, 4th ed. Upper Saddle River, NJ: Prentice Hall, 2003, p. 165.

[14] ANSYS, Inc., *ANSYS Release 10.0 Program Documentation*, 2005.

INITIAL DISTRIBUTION LIST

1. Defense Technical Information Center
   Ft. Belvoir, Virginia

2. Dudley Knox Library
   Naval Postgraduate School
   Monterey, California

3. Professor Young W. Kwon
   Naval Postgraduate School
   Monterey, California

4. Commandant (CG-5213)
   Attn: LCDR M. J. Simbulan
   U.S. Coast Guard
   Washington, DC

5. LT Robert P. Griffiths
   U.S. Coast Guard
   Washington, DC